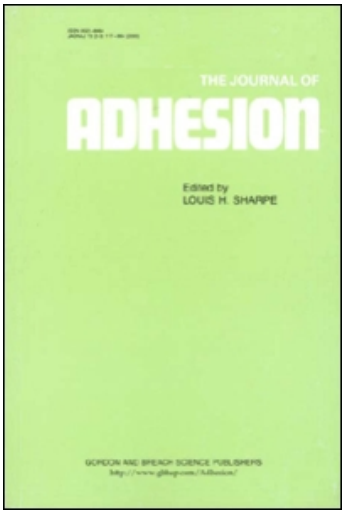

The Journal of Adhesion
Publication details, including instructions for authors and subscription information:
http://www.informaworld.com/smpp/title~content=t713453635

Adhesion of Graphite Fibers to Epoxy Matrices: I. The Role of Fiber Surface Treatment

Lawrence T. Drzal[a]; Michael J. Rich[b]; Pamela F. Lloyd[c]
[a] Air Force Wright Aeronautical Laboratories, Nonmetallic Materials Division, Mechanics and Surface Interactions Branch, AFWAL/MLBM, Wright-Patterson Air Force Base, WPAFB, OH, U.S.A. [b] University of Dayton Research Institute, Dayton, OH, U.S.A. [c] Systems Research Laboratory, Dayton, OH, U.S.A.

To cite this Article Drzal, Lawrence T. , Rich, Michael J. and Lloyd, Pamela F.(1983) 'Adhesion of Graphite Fibers to Epoxy Matrices: I. The Role of Fiber Surface Treatment', The Journal of Adhesion, 16: 1, 1 — 30
To link to this Article: DOI: 10.1080/00218468308074901
URL: http://dx.doi.org/10.1080/00218468308074901

J. Adhesion, 1982, Vol. 16, pp. 1–30
0021-8464/83/1601-0001 $18.50/0

Printed in Great Britain

Adhesion of Graphite Fibers to Epoxy Matrices: I. The Role of Fiber Surface Treatment

LAWRENCE T. DRZAL†

Air Force Wright Aeronautical Laboratories, Nonmetallic Materials Division, Mechanics and Surface Interactions Branch, AFWAL/MLBM, Wright-Patterson Air Force Base, WPAFB, OH 45433, U.S.A.

MICHAEL J. RICH

University of Dayton Research Institute, Dayton, OH 45469, U.S.A.

PAMELA F. LLOYD

Systems Research Laboratory, 2800 Indian Ripple Road, Dayton, OH 45440, U.S.A.

(*Received September 21, 1982; in final form December 11, 1982*)

Adhesion between graphite fibers and epoxy matrices is a necessary and sometimes controlling factor in achieving optimum performance. Manufacturers' proprietary fiber surface treatments promote adhesion without providing a basic understanding of the fiber surface properties altered through their use. This study has combined fiber surface chemistry, morphology, interfacial strength measurements and fracture characterization in order to elucidate the role of surface treatments. The results of this investigation lead to the conclusion that surface treatments designed to promote adhesion to epoxy matrix materials operate through a two-part mechanism. First, the treatments remove a weak outer fiber layer initially present on the fiber. Second surface chemical groups are added which increase the interaction with the matrix. Increases in fiber surface area are not an important factor in promoting fiber–matrix adhesion. In some cases the upper limit to fiber–matrix interfacial shear strength is the intrinsic shear strength of the fiber itself.

† To whom all correspondence should be addressed.

1. INTRODUCTION

The use of composite materials in aerospace applications is increasing because of the significant weight, cost and performance advantages these materials have over conventional structural materials. As the degree of sophistication of the aircraft designer increases, composite applications will be extended to a realm where current materials will not meet the load and environmental constraints efficiently. This will result in a two-fold requirement. First, composite properties which do not depend exclusively on the properties of the reinforcement, *i.e.*, off-axis properties, will become more important in composite structural design. Second, new generations of composite materials will be required where different fibers or matrices are needed to extend the operating environment of existing composites. In order to answer these needs a fundamental understanding of the fiber–matrix interphase and its effects on structure-property relationships in a composite is necessary.

Recent work has expanded the concept of the fiber–matrix interface which exists as a two-dimensional boundary into that of a fiber–matrix interphase that exists in three dimensions.[1]

The complexity of this interphase can best be illustrated with the use of a schematic model which allows the many different characteristics of this region to be visualized as shown in Figure 1.[2]

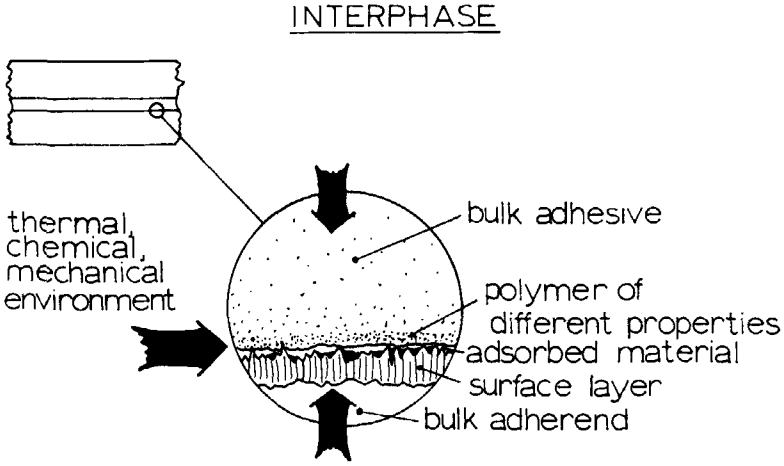

FIGURE 1 Schematic representation of the components of the three dimensional interphase between fiber and matrix.

The interphase exists from some point in the fiber where the local properties begin to change from the fiber bulk properties through the actual interface into the matrix where the local properties again equal the bulk properties. Components of this region can be identified. Many literature citations exist documenting this concept. The fiber may have morphological variations near the fiber surface which are not present in the bulk of the fiber.[3,4] The surface area of the fiber can be much greater than its geometrical value because of pores or cracks present on the surface.[5,6] The atomic and molecular composition of the fiber surface can be quite different from the bulk of the fiber.[7] Sufrace treatments can add surface chemical groups and remove the original surface giving rise to a chemically and structurally different region.[8] Exposure to air before composite processing can result in the adsorption of chemical species which may alter or eliminate certain beneficial surface reactivity. These adsorbed materials may also desorb at the increased temperatures seen in composite fabrication and be a source of volatiles which disrupt the interface if not removed.[9] Thermodynamic wetting of the fiber surface by the matrix is a necessary condition for fiber–matrix adhesion and is determined by the free energies of the components.[10] Both chemical and physical bonds exist at the interface and the number and type of each strongly influences the interaction between fiber and matrix. The structure of the matrix in the interphase can be influenced by the proximity of the fiber surface. Changes in reactivity due to adsorption of matrix components can alter the local morphology. Unreacted matrix components and impurities can diffuse to the interphase region altering the local structure.[11]

Each of these phenomena can vary in magnitude and can occur simultaneously in the interphase region. Depending on the system the interphase itself can extend from a few to a few thousand nanometers in depth. The structure of this region can have profound effects on the performance of the composite in terms of its mechanical strength, chemical and thermal durability.[14] The exact nature of this region must be understood if accurate predictive models of interphase behavior are to be developed and integrated into a model of composite performance. Because of the complexity of this region a need for a phenomenological approach has been recognized. Only when the exact nature of this region is understood will the interphase be considered as a material variable to be optimized in composite performance.

This paper presents the results of a program undertaken after

recognition of the complex nature of the composite interphase. This work is directed at developing the molecular understanding of the graphite fiber-epoxy interphase and the role of graphite fiber surface treatments in promoting fiber–matrix adhesion in composite materials.

2. PREVIOUS WORK

Complementary studies directed at quantifying the chemical and physical nature of the graphite fiber surfaces used in this investigation have been completed and published. The main points of these investigations which are necessary for a proper interpretation of the results of this program are summarized here.

A. Graphite fibers

Two graphite fibers were chosen as the representative fibers for this study. Both fibers were made from polyacrylonitrile and have mechanical properties which represent the practical extremes for fibers being used in composite materials. One fiber was graphitized at 1500°C and was designated as a type A fiber. The other was graphitized at 2600°C and was designated a type HM fiber. These treatments created fibers which differed in their tensile modulus. The A fiber has a tensile modulus of about 35 Msi (245 GPa) while the HM fiber has a value for the tensile modulus of 51 Msi (357 GPa).

The main structural elements of the fibers are graphitic ribbons which are oriented roughly parallel to the fiber axis. These ribbons are formed of graphitic crystallites which increase in size with increasing graphitization temperature (*i.e.*, 13 graphitic layers and 40 A wide for the 1500°C type A fiber to 20 layers thick and 70 A wide for the 2600°C type HM fiber). The ribbons twist and undulate along the fiber axis as shown schematically in Figure 2. The A fiber has less alignment and more twisting of the fibrils. This would produce a surface having not only graphitic basal planes but also corners and edges of the crystallites. The degree of order in the HM fiber is greater because of the higher graphitization temperature. The fibrils are well aligned and the surface of this fiber would be expected to have more basal planes and less corners and edges of the crystallites. Likewise, because of the greater basal plane alignment parallel to the surface

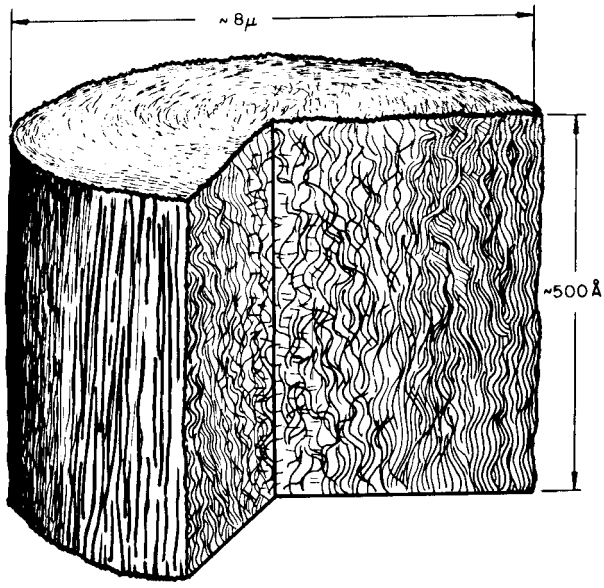

FIGURE 2 Schematic 3-D structural model of polyacrylonitrile based fiber with properties similar to type A (reference 12).

of the fiber, fiber shear strength would appear to be limited by the interbasal layer bonding. Detailed discussions of the structure of the fibers are available in the literature.[12]

These fibers were supplied by the manufacturer without any surface treatment and with a surface treatment designed to improve graphite fiber adhesion to epoxy matrices.[13] The surface treated fibers are designated AS and HMS and the untreated fibers are designated AU and HMU. Any other treatments given to the fibers are indicated with a label which appears after the fiber designation (*e.g.* 300°C VHT means a 300°C vacuum heat treatment).

B. Surface area

An increase in surface area is often the largest topographical change which occurs with fiber surface treatments designed to increase

adhesion. Krypton adsorption at temperatures between 100° and 120°K was used to determine the graphite fiber surface area and the change in area with surface treatment.

The surface area results indicated that no significant increase in surface area had taken place with surface treatment for either the A fiber or the HM fiber.[9,15] The surface areas of the A and HM fiber with or without surface treatment or subsequent thermal treatment were 0.45 and 0.51 meters squared per gram respectively.

C. Thermal desorption

The amount and composition of the thermal desorption products removed from the surfaces of the graphite fibers used in this study were measured at temperatures between 20° and 300°C.[9,15] Water, carbon monoxide and carbon dioxide were volatilized from both fibers at temperatures up to 200°C. If not properly removed during processing these species can serve as void generators within the composite. The amounts of material desorbed were the equivalent of one-half of a monolayer. These species were physisorbed material and not the chemisorbed surface groups added with fiber surface treatments.

D. Surface spectroscopy

X-ray Photoelectron Spectroscopy (XPS) or ESCA was conducted to provide atomic and molecular information about the graphite fiber surfaces selected for this study.[10] The data indicate that surface oxygen content more than doubles and the nitrogen content more than triples with surface treatment. Subsequent elevated temperature treatments in vacuum and with hydrogen (H) remove the surface oxygen and nitrogen. The highest temperature treatment with hydrogen, *i.e.*, 750°C successfully removes almost all of the elements except for a small amount of oxygen.

The HM fiber also increases its surface oxygen concentration with surface treatment (*i.e.*, HMU to HMS) by about a factor of two. No other elements were detected in significant quantities on the HM surfaces. Thermal vacuum treatments at temperatures of 300°C are effective in removing the oxygen species from this surface.

Other investigators have attempted to deduce the chemical functionality of the surface chemical groups detected on the fiber surface by ESCA. The most probable functionalities present are phenolic,

carboxylic, lactone and carbonyl groups.[8,16] Using peak assignments based on ESCA of other organic materials leads to the conclusion that the surface oxygen species were primarily carboxylic with a small amount of phenolic functionalities.[17] Ehrburger *et al.*[37] have determined the acid strength of groups on the surface of graphite fibers and have concluded that strong acidic groups have the largest effect on interfacial shear strength. Nitrogen present on the surface may be chemisorbed as a C-O-N complex.[18] Trace levels of other species are most probably present between the graphitic basal layers and not necessarily on the surface.

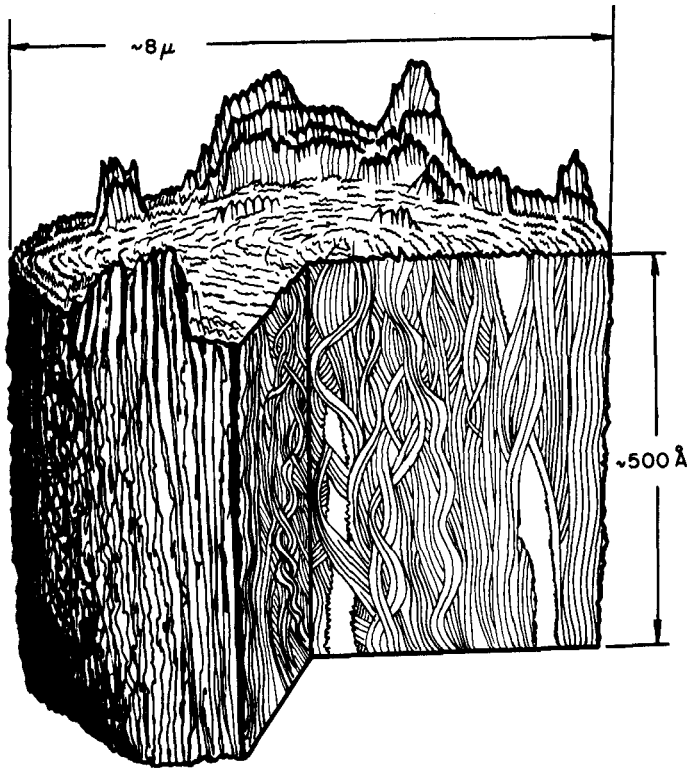

FIGURE 3 Schematic 3-D structural model of polyacrylonitrile based fiber with properties similar to type HM (reference 12).

E. Surface free energy

A necessary condition for fiber and matrix compatibility is thermodynamic wetting. This quantity can be measured through determination of the contact angle between fiber and matrix. Further insight into the specific interactions at the interface can be obtained by measuring the contact angle of a variety of liquids on the fiber surface each having different ratios of their polar to dispersive components of their surface free energies.[10]

A change in fiber surface free energy was detected for the surface treated fibers over the untreated fibers. The total surface free energy increases for both the AS and HMS fibers over their untreated precursors. The measured change is primarily in the polar component of the surface free energy.

The total surface free energy for each fiber is greater than or equal to that for the epoxy used in this study so that fiber wetting by the matrix will occur.

3. EXPERIMENTAL

A. Interfacial shear strength

A mechanical test capable of testing the fiber–matrix interphase under pure shear loading was required to assess the interactions occuring between fiber and matrix as a function of altered surface properties of the fiber. Composite design usually places the fiber–matrix interphase under shear loading but conventional composite testing methods evaluate a combination of types of loading as well as the synergistic effects of matrix and fiber on composite properties. This makes it difficult to delineate the effects of the interphase alone.

Single filament techniques are potentially less complex and lend themselves to application of pure loading modes. The commonly used fiber pullout technique has received wide useage with glass fibers but is difficult to use with the brittle and small graphite fibers of this study.[19] A technique used with metals was adapted for this study and designed to evaluate the interfacial shear strength directly.

A single graphite fiber is aligned axially in the cavity of a tensile dogbone coupon in a silicone mold. The desired matrix (in this case an epoxy) is cast around the fiber and the tensile coupon is loaded

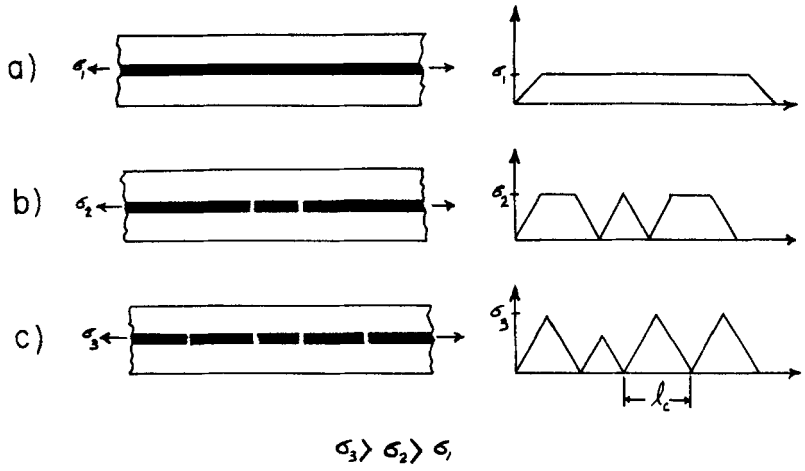

FIGURE 4 Fiber configuration and illustration of fiber fragmentation process during determination of interfacial shear strength.

in tension (Figure 4). As first proposed by Kelly[20] the matrix material which has a high strain to failure can be loaded in tension. The brittle fiber encapsulated within the coupon is loaded in tension through the transfer of shear forces from the coupon operating within the fiber–matrix interphase. The tensile loads on the fiber build up and exceed the fracture strength of the fiber causing it to fracture within the tensile coupon. This fiber fracturing process continues to create shorter and shorter fiber fragments until a length is reached which is no longer sufficient to support enough shear at the interphase and cause further fiber fracture. This limiting length is known as the critical transfer length l_c. A simple force balance assuming ideal fiber properties and uniform distribution of loads leads to the relationship

$$\tau = (\sigma_f/2)\,(d/l_c) \tag{1}$$

where d is the fiber diameter, σ_f is the fiber fracture strength at the critical length l_c and τ is the interfacial shear strength.

In practice a distribution of lengths is achieved due to the variations in fiber properties, *e.g.* defects, surface heterogeneities, geometric variations, etc. Therefore a statistical evaluation of the fiber length data must be made. This leads to a modified expression for

$$\tau = (\sigma_f/2\beta)\Gamma(1 - 1/a) \tag{2}$$

where Γ is the Gamma function and a and β are the Weibull shape and scale factors of the two parameter Weibull distribution.[21] The actual fragments lengths are measured and 'best fit' to a Weibull distribution with the aid of a computer.

B. Fiber fracture strength

Evaluation of Eq. (2) requires the values of the fiber fracture strength at the critical length. Since this length can often be a fraction of a millimeter, 25 mm gage length values can be misleading. In this study the fiber fracture strength at the critical lengths was determined directly through the use of a Tecam microtensile testing machine.[22] This device measures fracture stress directly through the use of an optical-mechanical method. The data in Table I shows that the fracture strength is significantly higher at the critical lengths than at the 25 mm gage lengths.

C. Photoelastic measurements

The single filament interfacial shear strength method has been used for glass fiber/polymer systems.[23] Fiber fragments lengths were measured after fracture through elimination of the matrix by combustion. Glass fiber fragments were then counted and measured microscopically. Because of some concern about fragment damage due to this process and the desire to obtain more information about the stress operating at the interphase, the sample lengths were measured directly on the stage of a microscope in the specimen as it was loaded. A hand operated tensile loading device was constructed[24] which kept the sample in place under the microscope and at the same time allowed the load to be increased incrementally. This had the advantage of allowing the fracture process to be observed directly. Critical length attainment could be verified before sample failure and fiber fragment lengths could be measured in-situ with the aid of a calibrated Filar eyepiece. Likewise with the use of transmitted polarized light the stresses occurring with the fiber–matrix interphase could be observed and recorded photographically. Qualitative differences in the stress pattern resulting from interphase changes could be observed. An Olympus BHA transmitted light microscope with polarizing attachment and long working distance objectives was

used for this purpose.[25] The polarizer and analyzer were set at extinction. Normal chromatic cycles were observed in the epoxy at low strains but disappeared at higher loadings. Fringes or chromatic variations were not observed under the high strain conditions present at the fiber fragment ends.

D. Microtoming

The 25 mm gage section of the 62.5 mm long by 3 mm wide by 1.5 mm thick tensile coupon containing the embedded fiber also contained information about the mode of fracture within the interphase. Conventional optical microscopy could not discriminate events at the resolution level required. Scanning Electron Microscopy could not penetrate into the specimen. Ultramicrotoming offered the possibility of examining the interphase directly under the high magnification capabilities of the Transmission Electron Microscope (TEM).

1.5 mm segments were cut from the tensile coupon gage length section of both unstrained and strained samples. They were trimmed to trapezoidal shape and were mounted in an ultramicrotome[26] with the fiber axis parallel to the diamond blade. Sections were obtained with a 55 degree diamond knife with fiber orientation a few degrees off the fiber axis. 60 to 90 nm thick sections were cut progressively through the sample. These sections were floated onto a water bath and picked up onto 200 mesh formvar coated grids.[27] They were dried on filter paper and stored in a vacuum dessicator until TEM observation.

The grids were placed directly into a JEOL-100CX TEM for viewing.[28] Figure 5 is a typical TEM photomicrograph of a section of a graphite fiber–epoxy specimen sectioned through the interphase by this process. The knife direction in this and all succeeding microtomed photomicrographs is perpendicular to the fiber–matrix interphase. The homogeneous featureless region is the epoxy while the textured area is the graphite fiber thin section. The sample was not strained before sectioning and the fiber–matrix interphase comes through the sectioning process intact. Each fiber–matrix combination was sectioned prior to straining to verify that interfacial artifacts from the sectioning process are not induced in the sample. All TEM micrographs were taken at 100KV. Sections included in this report are representative of features observed for each fiber–matrix combination.

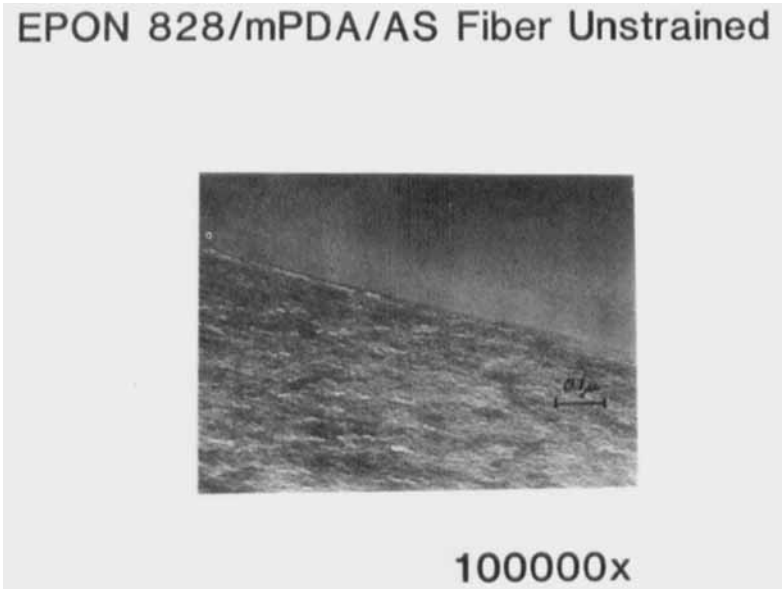

FIGURE 5 Transmission Electron Micrograph (TEM) of an ultramicrotomed section of an AS fiber-EPON 828/mPDA interface before straining illustrating the preservation of the integrity of the interface with sample sectioning.

E. Matrix

An epoxy matrix was chosen for this study to model structural matrix materials without including the complexity of the commercial chemical formulations.[29] Epon 828[30] cured with the stoichiometric amount of meta-phenylene diamine (mPDA) of 14.5 phr[31] was selected as the matrix material. A master batch of both components was obtained. It was stored under dark, dry conditions to eliminate deterioration or contamination with time.

A cure cycle and processing cycle were established and followed rigorously throughout this study. Both Epon 828 and mPDA were weighed in separate containers and heated to 65°C to melt the mPDA. The components were mixed, debulked for two minutes at full vacuum and poured into silicone molds containing the aligned fibers. The molds were processed two hours at 75°C and two hours at 125°C followed by a slow overnight cooldown. Since gelation occurs during the lower temperature cycle, residual stresses resulting from cure shrinkage were kept to a minimum.[32]

4. RESULTS

A. Interfacial shear strength

Table I contains a summary of the results obtained from the interfacial shear strength determinations. Column 1 lists the fibers and their specific treatments. Comparing the fiber fracture strengths at 25 mm gage length with the values obtained at the critical lengths (Columns 4 and 5) shows that the fracture strengths increase with shorter fiber gage length. This has been noted in the literature and log-log or log-semi-log relationships have been proposed.[33,34] Column 2 is the critical length to diameter ratio determined from a computer fit of the fragment data to a two parameter Weibull function. Column 3 is a tabulation of the coefficient of variation of the critical length to diameter ratio based on the mean value of the mean length for each coupon. Column 6 lists the Weibull shape parameters for the entire sample population.

TABLE I
Interfacial Shear Strengths

			σ_f(25 mm)		$\sigma_f(l_c)$			τ	
Fiber	l_c/d	c.v.	ksi	GPa	ksi	GPa	a	ksi	MPa
AU	108	0.16	379	2.61	581	4.00	3.3	3.50	24.1
AS	41.7	0.10	429	2.96	681	4.69	3.3	10.7	74.0
AS (300°C)	43.6	0.18	424	2.92	645	4.45	2.8	10.4	71.7
AS (600°C)	37.2	0.07	350	2.41	580	4.00	3.6	9.87	68.0
AS (750°C/H)	46.1	0.19	293	2.02	630	4.35	2.7	9.54	65.8
HMU	143	0.14	364	2.51	468	3.23	3.7	2.02	13.9
HMS	118	0.14	360	2.48	522	3.60	3.2	2.94	20.3
HMS (300°C)	122	0.14	325	2.24	535	3.69	3.3	2.86	19.8

The value of the critical length to diameter ratio listed in Column 2 represents the experimentally observed parameter. However, note must be made of the fracture events which occur near the critical length. As the fiber fragment lengths approach the critical length some fragments will be slightly longer and some just slightly less than the critical length. Those shorter fragments will no longer fracture but those just slightly greater will fracture again giving fragments approaching one half of the critical length. Therefore fragment lengths are expected

which would be distributed between the critical length and one-half of the critical length. The experimentally determined value would then be the median value in this interval.

Column 7 lists the interfacial shear strength. The interfacial shear strength values are sensitive to and reflect the changes detected within the fiber–matrix interphase due to changes in the fiber surface. Comparing the A fibers among themselves highlights the changes occurring as a result of surface treatments. The untreated AU fiber gives an initial value for the interfacial shear strength of 3.50 ksi. The value for the interfacial shear strength on this same fiber after surface treatment (AS) increases by a factor of three. The surface composition and energetic analysis of this fiber showed that oxygen and nitrogen concentration on the AS surface is increased by a factor of two over the AU fiber and that the surface behaves in a more polar manner. The values of interfacial shear strength determined for the other AS fibers which have been treated in various ways to reduce the surface oxygen content decrease with decreasing surface oxygen from the value determined for the AS fiber. The value of the interfacial shear strength for the hydrogen reduced fiber surface even though its surface content of oxygen is much less than that for the untreated AU fiber, is still greater than that of the untreated AU fiber (9.54 ksi *vs* 3.50 ksi) although less than that for the surface treated AS fiber (10.7 ksi).

The HM fibers display trends similar to that seen for the A fibers. The untreated HMU fiber gives a value of interfacial shear strength lower than that detected for any other fiber (2.02 ksi). Its surface oxygen content is also very low. Surface treatment to form HMS causes a substantial increase in interfacial shear strength from 2.02 ksi to 2.94 ksi. This is about a fifty percent increase and corresponds with about a two fold increase in surface oxygen as detected by the ESCA measurements. Removal of surface oxygen through a 300°C thermal/vacuum treatment again reduces the interfacial shear strength but not to the level of the untreated HMU filter (2.86 ksi *vs* 2.02 ksi) even though the oxygen level is below that of the HMU fiber.

B. Interfacial stress and fracture

Type A fiber The stresses generated within the fiber–matrix interphase are altered with changes in fiber surface treatment. The mode of fracture between fiber and matrix is altered with surface treatment as

well. The photoelastic stress pattern observed in each specimen was recorded photographically with increasing strain. A collage of these observations at 400x and increasing values of strain was compiled. Figure 6 shows the photoelastic data for the AU fiber in the epoxy matrix. The values of strain accompanying the figure are measured from machine displacement and only indicate the relative changes from one picture to the next. The absolute values of strain would be expected to be smaller than these machine values. At low strains after a

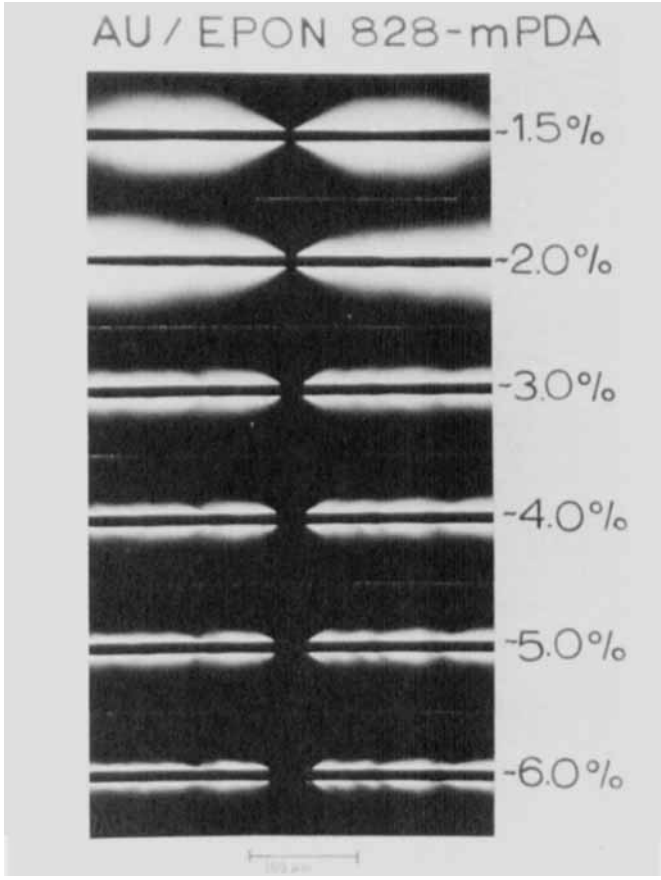

FIGURE 6 Polarized Transmitted Light Micrograph of the AU fiber-EPON 828/mPDA interface at a fiber break and its alteration with increasing strain.

fiber break an intense photoelastic region appears around the ends of the fiber. With increasing strain this region rapidly expands down the fragment away from the break. Dynamic observation of this process suggests that the stresses proceed along the fragment by a stick-slip mechanism. That is the stresses build up then appear to release and move ahead an incremental amount repetitively. This results in a stress pattern that has alternating light and dark areas in the micrographs at the points where the stress pattern "jumped" ahead. For this particular fiber–matrix combination, each fiber fragment fails interfacially at very low strains. With increasing tensile load, the fiber fragments interact with the matrix only through weak frictional forces. The interfacial shear strength is very low and the fiber exerts very little reinforcing effect on the matrix. Under axial tension, the matrix can extend without being constrained by the presence of the fiber. This results in the gap between fragments extending in length with increasing strain. Subsequent observation of fibers with higher interfacial shear strength shows that this fragment separation is retarded by the presence of a well-bonded fiber.

Ultramicrotomed sections of this specimen document the mode of interfacial fracture taking place. Figure 7 is a TEM photomicrograph of the AU/epoxy interface after straining. The entire interphase has failed and the sectioned specimens show a typical region where separation of the epoxy from the graphite fiber has taken place. Close inspection of these photomicrographs reveals that many small fragments of graphite fiber have been removed to the epoxy side of the fracture path. This suggests that the fracture path was one that involved propagation through the outer layers of the AU fiber as well as interfacial failure between the fiber and epoxy. Many small fragments of graphite fiber can be seen strongly adhering to the epoxy side of the failure path confirming that failure of a weak fiber outer layer is a major element in interfacial fracture of this fiber matrix combination.

The surface treated fiber (AS) behaves much differently under polarized light than the untreated AU fiber. Figure 8 shows that at the fiber break the stresses immediately build up at the ends of the fiber. With increasing strain however, a narrow very intense photoelastic region remains around the fiber while the initial bulbous region moves away from the fiber ends and toward the center of the fragment. The interfacial shear strength measured for this system is over a factor of three greater than for the AU fiber indicating a much greater degree

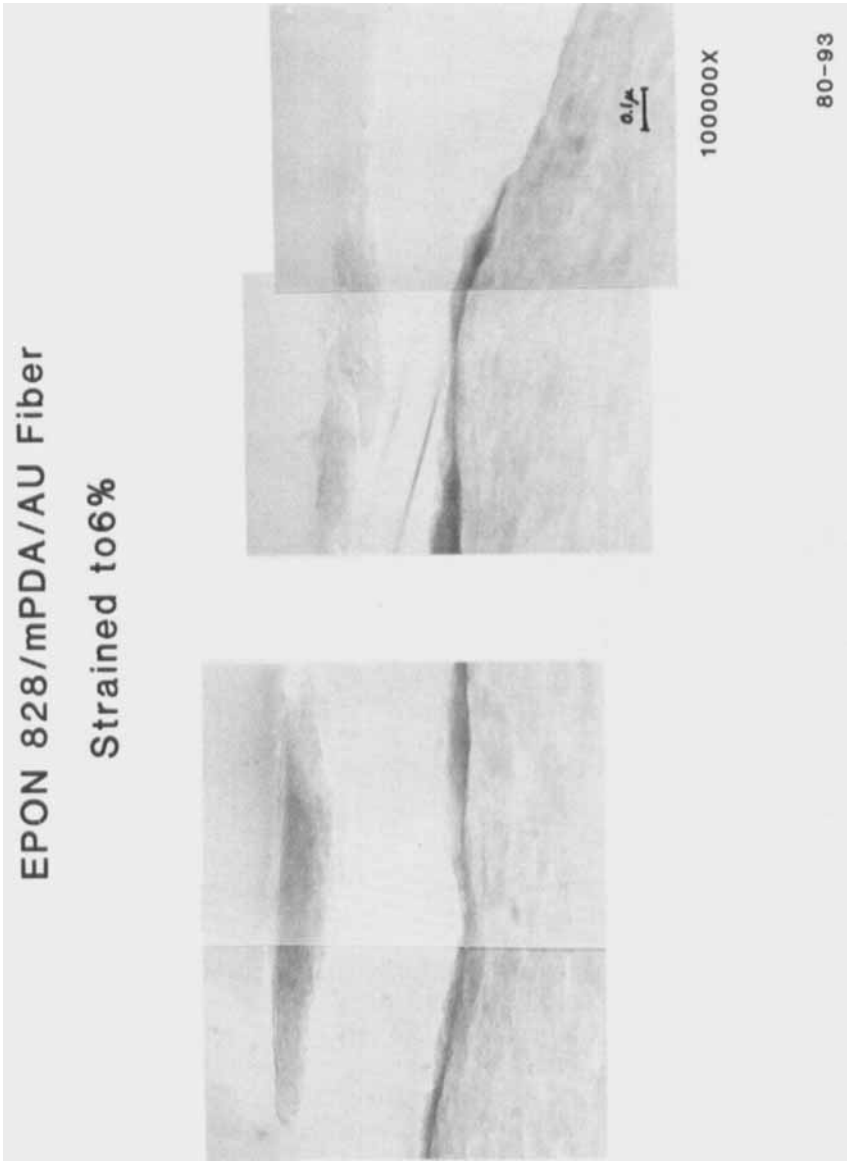

FIGURE 7 Transmission Electron Micrograph (TEM) of an ultramicrotomed section cut parallel to the fiber axis of the AU fiber-EPON 828/mPDA interface after straining to 6%.

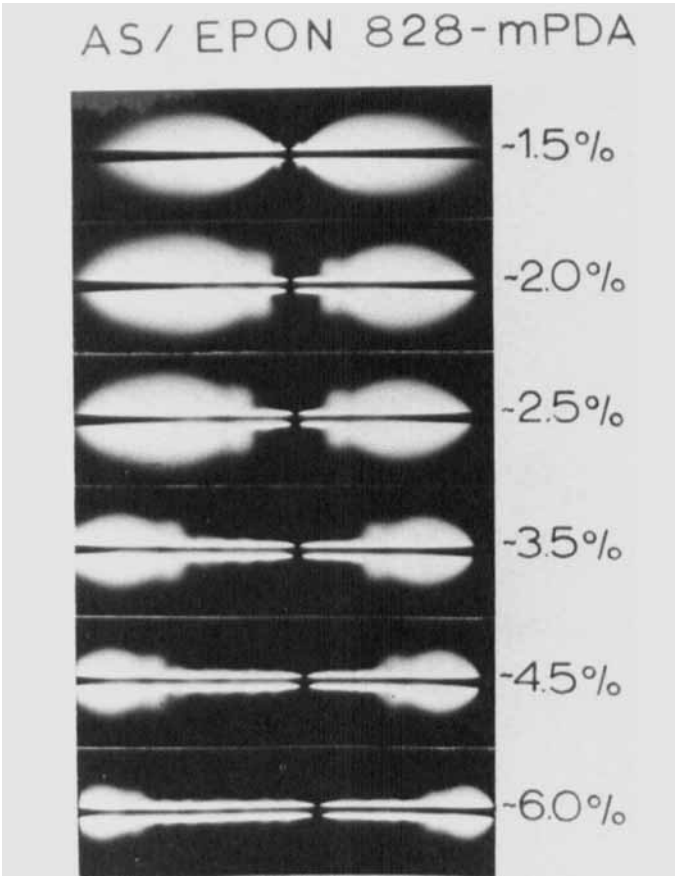

FIGURE 8 Polarized Transmitted Light Micrograph of the AS fiber-EPON 828/mPDA interface at a fiber break and its alteration with increasing strain.

of fiber–matrix interaction. Indeed, the separation at the fiber break remains relatively constant with increasing strain while for the AU fiber the gap between segments widens appreciably.

The ultramicrotomed sections of this sample document the propagation of an interfacial crack emanating from the fiber fragment ends and progressing along the fragment (Figure 9). Comparison of this photomicrograph with the photoelastic stress patterns suggests that the narrow intense stressed area that remains around the fiber is a region

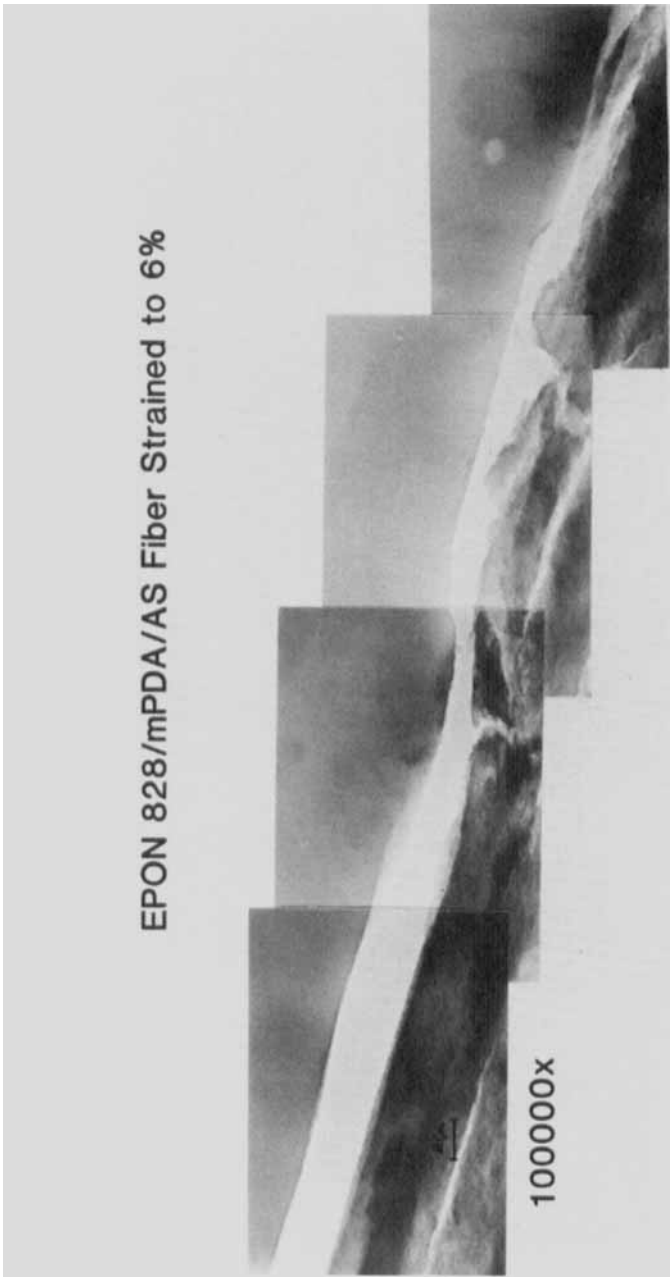

FIGURE 9 TEM of an ultramicrotomed section of the AS fiber-EPON 828/mPDA interface after straining to 6%.

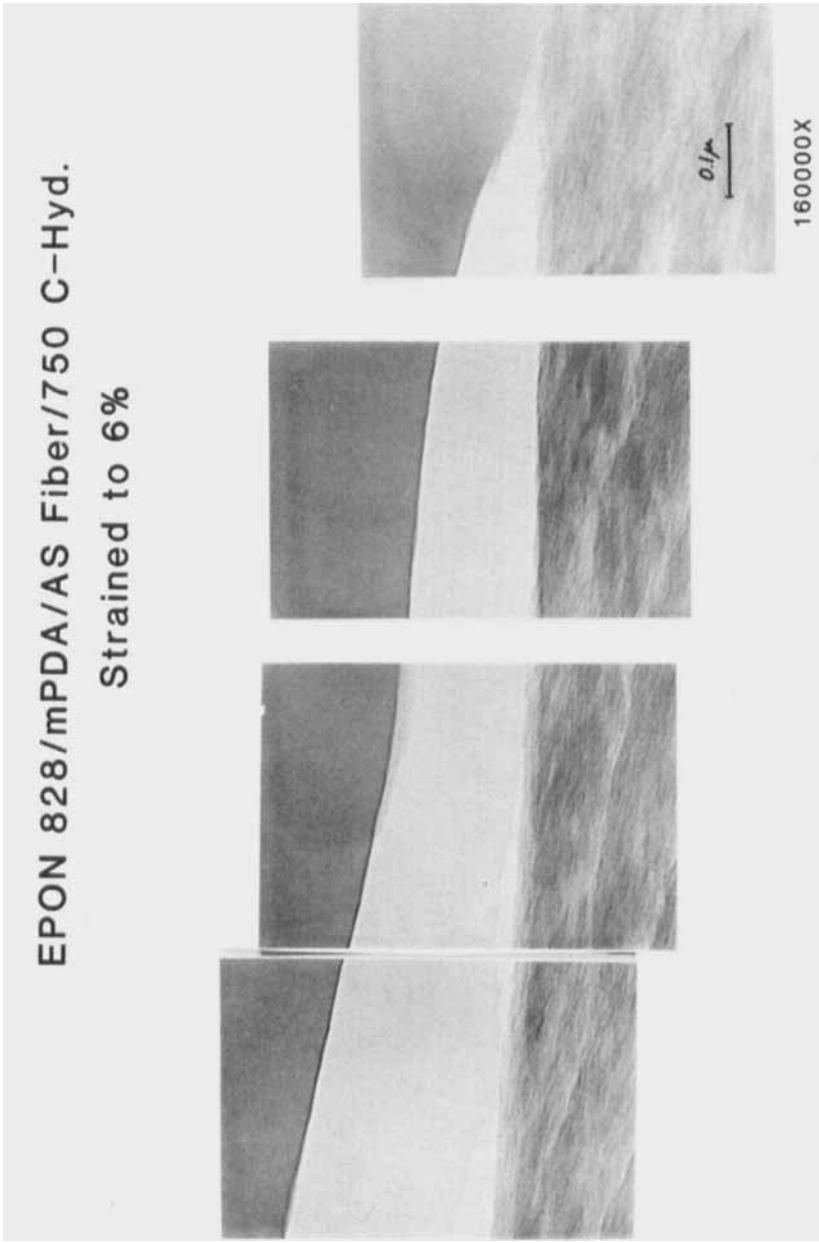

FIGURE 10 TEM of an ultramicrotomed section of the AS (750°C/H) fiber-EPON 282/mPDA interface after straining to 6%.

where an interfacial crack has passed while the bulbous region at the tip of the photoelastic region appears to be the plastic zone associated with the moving crack tip. The fracture path appears to be strictly interfacial with no evidence of graphite fiber fragment pullout to the epoxy side as observed with the AU sample.

The photoelastic behavior of the AS fibers with decreasing amounts of surface oxygen groups was identical to that shown in Figure 8 for the AS fiber. The critical lengths increased and the value of the interfacial shear strength therefore decreased. The shape of the stress pattern, the movement of it away from the fiber break, the lack of movement of the fiber fragments, etc. were nearly identical to the observations made on the AS fiber.

The ultramicrotomed sections of these samples were also identical to those observed for the AS fiber. Figure 10 is a TEM photomicrograph of a section of the hydrogen reduced AS (750°C/H) fiber in the same epoxy. A strictly interfacial fracture path is detected between fiber and matrix just as in the AS fiber case with no detectable graphite fiber fragments observed attached to the epoxy side of the fracture path.

Type HM fiber The photoelastic stress patterns observed for the HM fibers are very similar to that observed for the AU fiber. The patterns recorded with increasing strain are shown in Figure 11. Immediately after a fiber break the ends of the fragments are highly stressed and the stresses redistribute themselves along the fragment length. The dynamics of this process again show a "stick-slip" type of propagation of the stress pattern along the fiber fragment away from the break giving rise to the alternating light and dark regions. The gap between fragments increases with increasing strain.

The TEM micrographs (Figure 12) of the ultramicrotomed sections of this sample show that the fracture path is interfacial with fragments of the graphite surface being pulled off to the epoxy side of the fracture. The density of fragments is quite high all along the fracture interface.

Surface treatment of the HM fiber to produce the HMS fiber promotes a higher degree of interfacial shear strength. The photoelastic stress patterns of this specimen (Figure 13) show a slight qualitative difference from the HMU fiber pattern. The stresses are more uniform and the gap between fragment ends does not increase as rapidly with increasing strain as for the HMU. However, overall

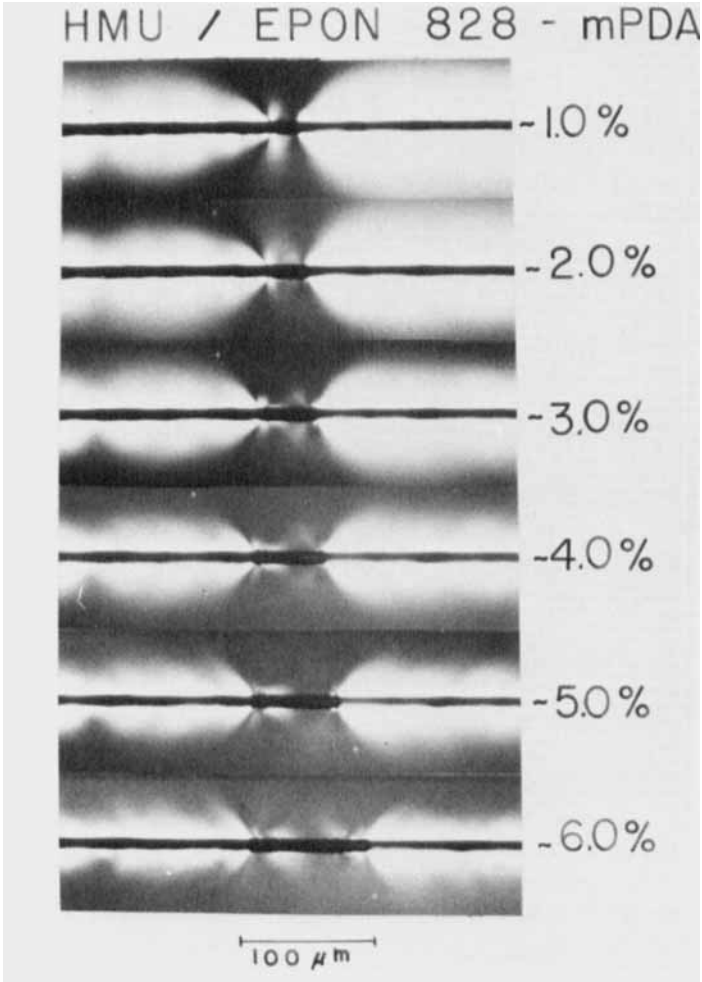

FIGURE 11 Polarized Transmitted Light Micrograph of the HMU fiber-EPON 828/mPDA interface at a fiber with increasing strain.

the stress pattern is very similar in appearance and dynamic behavior.

The TEM micrographs (Figure 14) of the sectioned surface treated HMS fiber specimens however show that the fracture path still includes the failure of sections of the outer layers of the graphite fiber and adherence of those fragments to the epoxy side of the

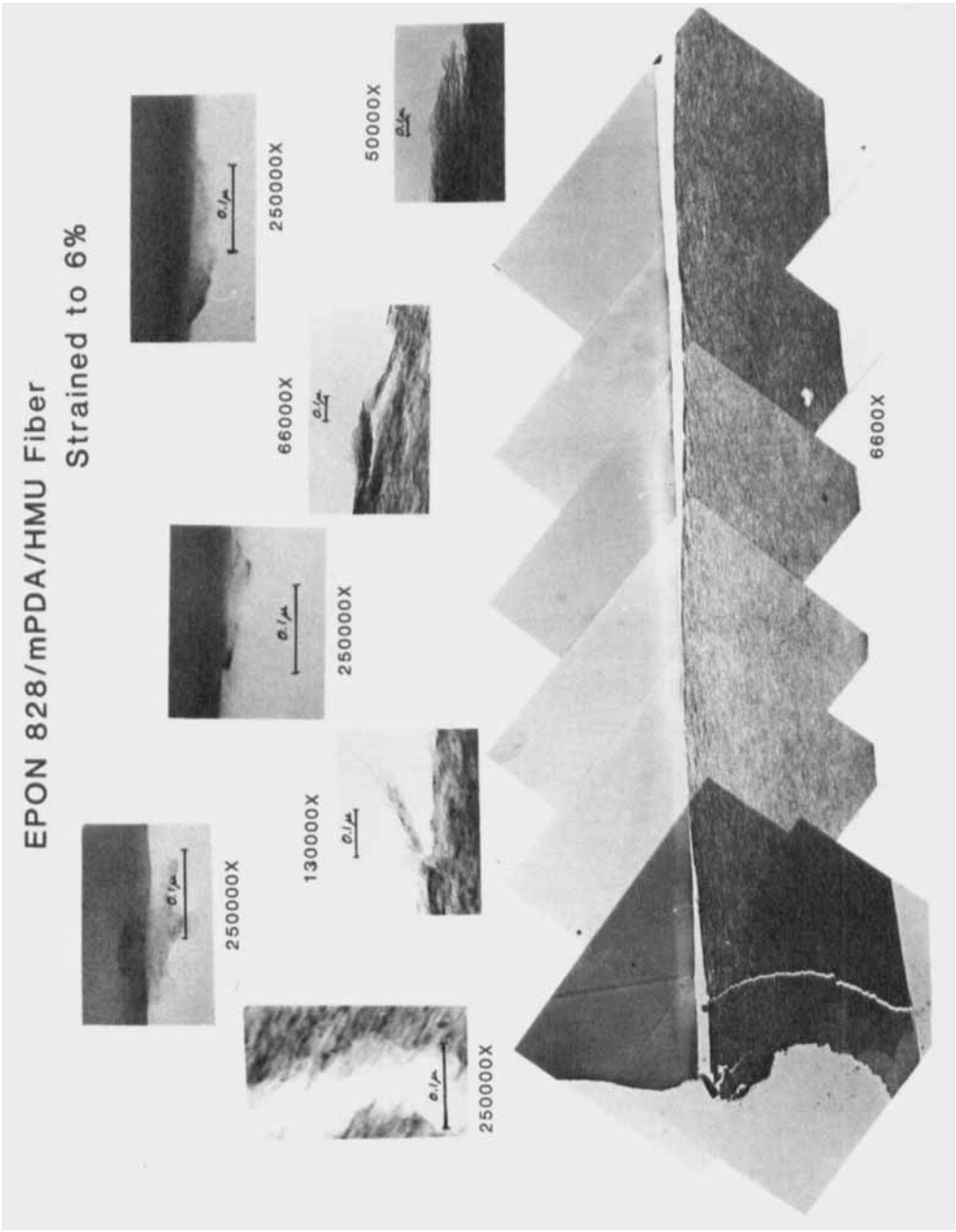

FIGURE 12 TEM of an ultramicrotomed section of the HMU fiber-EPON 828/mPDA interface after straining to 6%.

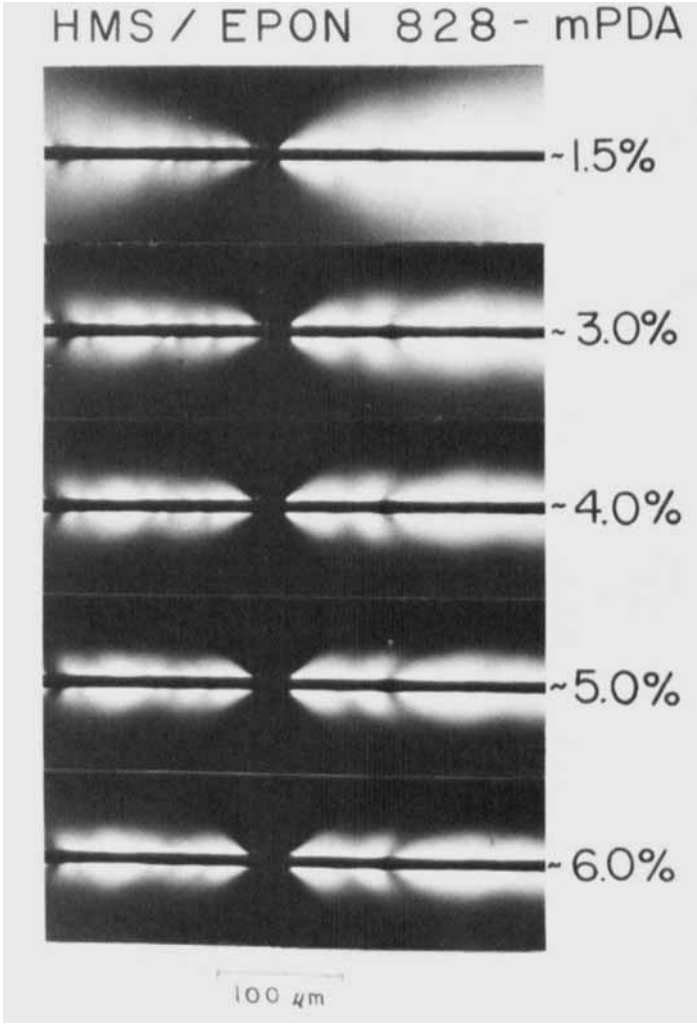

FIGURE 13 Polarized Transmitted Light Micrograph of the HMS fiber-EPON 828/mPDA interface at a fiber break with increasing strain.

fracture. Qualitatively the density of fragments is less than that of the HMU fiber.

The HMS (300°C) sample which has had most of the oxygen groups removed with thermal/vacuum treatment behaves very similarly to the HMS fiber. The photoelastic stress pattern and the TEM sections are

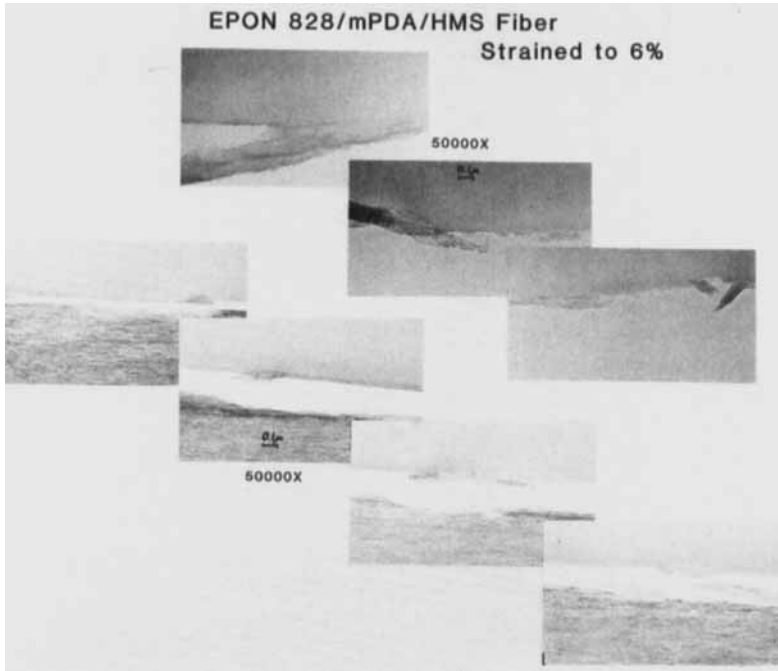

FIGURE 14 TEM of an ultramicrotome section of the HMS fiber-EPON 828/mPDA interface after straining to 6%.

indistinguishable from the HMS fiber data. That is, the fracture path is again interfacial with fragments of the graphite remaining on the epoxy side indicating that the failure path involved fracture in the outer layer of the fiber.

5. DISCUSSION

The relationships between the parameters that are investigated in this study which explain the interaction between fiber surface chemistry, the effect of fiber surface treatment on fiber surface chemistry and their relationship to fiber–matrix interfacial shear strength are illustrated most effectively by plotting the interfacial shear strength against the fiber surface oxygen content. (Inclusion of atomic species other than oxygen or the use of the polar component of the fiber surface free

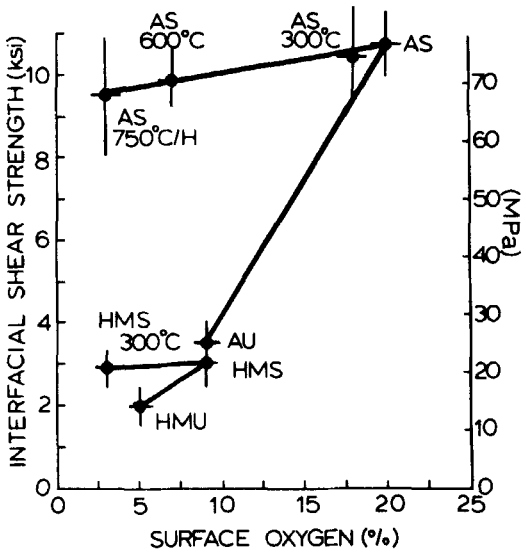

FIGURE 15 Interfacial shear strength plotted as a function of surface oxygen concentration determined by ECSA for the type A and HM fibers.

energy does not alter the trends of the graph or the conclusions to be drawn therefrom). This plot is displayed in Figure 15.

The data falls into two regions on the graph. The A fiber data lies in the upper portion and the HM fiber data in the lower portion. The A fiber data leads to the conclusion that two separate surface treatment mechanisms are operating. This can be seen by comparing the data starting at the AU fiber data point.

Surface treatment which converts the AU to AS fiber doubles the oxygen content and causes the interfacial shear strength to rise to a value over three times that of the AU. However, removal of the surface oxygen groups with the various treatments (*i.e.*, AS (300°C), AS (600°C) and AS (750°C/H) to the AS decreases the value obtained for the interfacial shear strength below that obtained for the AS but still above the value obtained for the AU. Some other change occurred with surface treatment which allows a higher value of interfacial shear strength to be retained even after the surface oxygen groups are removed. Kalnin[35] in a review of graphite fiber surface treatments proposes that the surface oxidative treatment processes not only add

surface chemical groups but also remove some of the outer atomic layers from the fiber surface.

Fitzer[36] and Thomas[18] in work with phenolic matrix carbon fiber composites have inferred an effect on surface morphology. The work documented here which combines the photomicrographs of the fractured interface with the interfacial shear strength and stress patterns show that indeed a two part effect results from fiber surface treatment. There is a mechanical effect due to the removal of the original weak boundary layer and a surface chemical effect due to the addition of surface chemical groups which interact more strongly with the epoxy.

As the fiber goes through its processing cycle while it is being converted from polyacrylonitrile to graphite the same surface which is in contact with the reactive environments and high temperature becomes the fiber surface. It is reasonable to expect that this surface is very defect laden and might constitute a "weak boundary". Under shear loading in a matrix, interfacial failure at low loads involving separation of the first few fiber layers from the bulk of the fiber is observed due to the inability of this layer to withstand high shear loads on this AU fiber surface. Surface treatment not only adds oxygen groups but also removes this defect laden layer leaving behind a structurally sound surface able to withstand higher shear loading and which has more surface chemical groups capable of interacting with the epoxy. Failure between the epoxy and this AS fiber surface becomes interfacial with no observable fiber failure since the outer weak layer has been removed. The fiber surface treatments which removed oxygen from the AS fiber surface decreased the interaction with the epoxy but did not affect the ability of the defect free surface layer to sustain higher shear loads than the AU fiber surface even though their chemical interaction with the epoxy was reduced. They therefore gave higher values of interfacial shear strength. For this epoxy matrix and this fiber surface treatment, the surface chemical effect responsible for the increase in interfacial shear strength between the AS fiber and the A fiber without surface chemical groups—AS (750°C/H) can be estimated to be 16%. The effect of removing the defect laden surface is responsible for the change in interfacial shear strength between the AU fiber and the AS (750°C/H) *i.e.*, 84%.

The HM fiber data parallel the behavior of the A fiber. The HMS surface treated fiber has more oxygen and some of the weak outer layer has been removed with the surface treatment. This layer for the HM fiber is much thicker than for the A fiber because of

the higher processing temperature used with this material.[12] In addition because of the more graphitic nature of the HM fiber and the better alignment of the fibrils the fiber would be expected to be able to withstand a lower level of shear loading than the A fibers. The fracture micrographs support this explanation and show failure in the outer fiber layers for all HM fibers. The highest value of interfacial shear strength attainable for the HMS fiber is very low, *i.e.*, 2.94 ksi. The shear strength between layers of commercial graphite has been estimated to be about 3.00 ksi.[8] Therefore the upper limit for Type HM fibers may have been reached and may be the shear strength between basal planes. After the surface chemical groups are removed from the HMS fiber the value of the interfacial shear strength does not decrease to the value for the untreated HMU fiber indicating that the fiber surface after treatment is structurally sounder and capable of sustaining higher shear loading although not as high a level as for the A fiber. The contribution to the interfacial shear strength due to the surface chemical effect can be estimated as due to the change in interfacial shear strength between the HMS and HMS (300°C) fibers, which for this combination is very small. The contribution due to removal of the weak outer surface would be represented by the difference between the HMU and HMS (300°C) fiber, *i.e.*, $> 90\%$.

The contribution to the interfacial shear strength due to the specific chemical interactions between these A and HM graphite fibers and this EPON 828-mPDA epoxy matrix is small. The contribution to the interfacial shear strength from specific chemical interactions could, however, gain more importance if the fiber surface chemistry and/or chemical nature of the polymeric matrix is changed.

6. CONCLUSIONS

In summary, the following general conclusions about the effect of graphite fiber surface treatments on fiber–epoxy matrix shear strength can be made:

Graphite fiber oxidative surface treatments tend to increase fiber–matrix shear strength with epoxies through a two part mechanism. First an outer weak defect laden fiber surface layer is removed. This results in a surface which is capable of supporting higher shear loadings. Second, surface oxygen groups are added which can interact with the

polar epoxy matrix contributing to higher fiber–matrix interfacial shear strength.

In addition, oxidative surface treatments do not operate through an increase in fiber surface area. For the case of high modulus fibers, high shear loads can not be sustained because of intrinsic limitations due to their morphological make-up. The upper limit in shear may be the shear strength between graphite basal layers.

Acknowledgements

The authors are grateful to Mr. K. Lindsay of UDRI for the graphite fiber tensile strength data measurements at the critical length and to Mr. D. Hall of UDRI for the hydrogenation treatment of the graphite fibers.

References

1. L. H. Sharpe, *J. Adhesion* **4**, 51 (1972).
2. L. T. Drzal, *The Role of the Polymer–Substrate Interphase in Structural Adhesion*, AFML-TR-77-129 (1977).
3. R. Bacon and A. F. Silvaggi, *Carbon* **9**, 321 (1971).
4. A. Fourdeus, R. Perret and W. Roland, *General Structural Features of Carbon Fibers—Their Composites and Applications* (London, 1971).
5. V. J. Mimeault and D. W. McKee, *Nature* **224**, 739 (1969).
6. V. J. Mimeault, *American Chemical Society Polymer Preprints* **31**, 479 (1971).
7. F. Hopfgarten, *Fibre Science and Technology* **12**, 283 (1979).
8. J. V. Larsen, T. G. Smith and P. W. Erickson, *Carbon Fiber Surface Treatments* NOLTR-71-165 (1971).
9. L. T. Drzal, *Carbon* **15**, 129 (1977).
10. G. E. Hammer and L. T. Drzal, *Appl. Surf. Sci.* **4**, 340 (1980).
11. J. L. Tacich and J. A. Koutsky, *Chemistry and Properties of Crosslinked Polymers*, S. Labana, ed. (Academic Press, NY, 1977), p. 303.
12. R. J. Diefendorf and E. W. Tokarsky, *The Relationship of Structure to Properties in Graphite Fibers* AFML-TR-72-133 (1977).
13. Hercules, Inc., Wilmington, DE.
14. J. L. Kardos, *Trans. N.Y. Acad. Sci., Ser II.* **35**, 136 (1973).
15. L. T. Drzal, J. A. Mescher and D. Hall, *Carbon* **17**, 375 (1979).
16. B. Rand and R. Robinson, *Carbon* **15**, 257 (1977).
17. D. M. Brewis *et al.*, *Fibre Science and Technology* **12**, 41 (1979).
18. C. R. Thomas and E. J. Walker, *5th London International Conference on Carbon and Graphite*, 520 (1978).
19. L. J. Broutman, *Proc. Ann. Tech. Conf. of RP/Composites Inst., The Society of Plastics Ind.* **25**, Paper 13-B (1970).
20. A. Kelly, *Proc. Royal Soc. A.* **319**, 95 (1970).
21. A. C. Cohen, Jr., *Technometrics* **7**, 579 (1978).
22. Tecam Instruments, Techne (Princeton) Limited, Princeton, NJ, U.S.A.
23. W. A. Fraser, F. H. Ancker and A. T. DiBenedetto, *Proc. of 1975 Conf. of RP/Composites Inst.*, Paper 22A, (1975).

24. L. T. Drzal *et al., Proc. of 1980 Conf. of RP/Composites Inst.*, Paper 20-C (1980).
25. Olympus Corp of America, New Hyde Park, NY, U.S.A.
26. E. I. duPont Co., Wilmington, DE, U.S.A.
27. Ladd Research Industries, Inc., Burlington, VT 05402, U.S.A.
28. JEOL Inc., Medford, MA, U.S.A.
29. D. K. Hadad, J. S. Fritzen and C. A. May, *Exploratory Development of Chemical Quality Assurance and Composition of Epoxy Formulations*, AFML-TR-77-217 (1978).
30. Shell Chemical Company, Houston, TX, U.S.A.
31. H. Lee and K. Neville, *Handbook of Epoxy Resins*, McGraw-Hill, NY, (1967).
32. K. Fisch and T. Hoffman, "Reaction Mechanisms, Chemical Structures and Changes in Properties during the Curing of Epoxy Resins" *Plastic Tech.* (1961).
33. P. E. McMahon, *SAMPE Quarterly* **6**, 7 (1974).
34. S. Chwastiak, J. B. Barr and R. Didchenko, *Carbon* **17**, 49 (1979).
35. I. L. Kalnin, *Proc. 1st USA–USSR Symposium on Fracture of Composite Materials, Riga, USSR*, G. Sih and V. P. Tamuszs, eds. (Sijthoff and Noordhoff, Amsterdam, 1979), p. 373.
36. E. Fitzer *et al., Carbon* **18**, 389 (1980).
37. P. Ehrburger, J. J. Herque and J. B. Donnet, *5th London International Conference on Carbon and Graphite*, 398 (1978).